Research Article
doi.org/10.1002/cplu.202300045

Chemistry Europe
European Chemical Societies Publishing

www.chempluschem.org

Fiber Spinning of Ultrahigh Molecular Weight Isotactic Polypropylene: Melt Spinning and Melt Drawing

Lucas Stieglitz,[a] Christina Geiger,[b] Paula F. Großmann,[a] Moritz Kränzlein,[a] Katia Rodewald,[a] Peter Müller-Buschbaum,[b, c] and Bernhard Rieger*[a]

Herein, this work reports fiber spinning of tailored isotactic polypropylene (iPP) by melt spinning and melt drawing, yielding an adjustable diameter of 40–400 μm. The crystallinity of all obtained fibers with a molecular weight between 330–1400 kg/mol is increased by thermal annealing and investigated *via* differential scanning calorimetry (DSC) as well as wide angle X-ray scattering (WAXS). The potential of ultrahigh molecular weight iPP (UHMW-iPP) fibers compared to fibers manufactured from industrially available iPP becomes evident when the mechanical performance is compared: fibers spun from UHMW-iPP (1400 kg/mol) enable a tensile strength of up to 400 MPa, whereas commercially available fibers (330 kg/mol) show a tensile strength of approximately 50 MPa. However, UHMW-iPP exhibits a short timeframe, in which extrusion is possible, thereafter extrusion rupture occurs, probably induced by an increased melt viscosity.

Introduction

Tailoring isotactic polypropylene (iPP) was first made possible by Brintzinger and Kaminsky with their discovery of the isospecific *ansa*-metallocene catalyzed polymerization of propylene in 1985.[1] In the following years, macromolecular characteristics, such as molecular weight, degree of isotacticity and melting transition were adjusted by a variation of the basic group (IV) metallocenes' scaffold.[2] By using the ultrarigid hafnocene dichloride **II** (Figure S45), Rieger *et al.* isolated in 2012 perfectly isotactic PP with the so far highest molecular weight of up to 5800 kg/mol and melting transition *ex reactor* at 171 °C – this iPP remains until today as the benchmark iPP in terms of macromolecular characteristics.[2a] Recently, an improved polymerization procedure was established to tremendously increase this polymer's yield per utilized ligand system by avoiding the tedious *rac/meso* separation.[3]

Compared to polyethylene (PE), iPP has some serious advantages: an almost 25 °C higher melting transition, a higher tensile strength and impact resistance as well as a lower mass density.[4] Therefore, ultrahigh molecular weight iPP (UHMW-iPP) fibers potentially could outperform UHMW-PE *Dyneema* fibers. However, the processing of UHMW polymer fibers *via* the classic melt extrusion route is considered very challenging and even a few claim it to be nearly impossible.[4] This is mainly attributed to the high melt viscosity, which correlates with the polymer's molecular weight with $\eta_0 \propto M_w^{3.4}$.[5] To circumvent this, a few attention was directed onto the gel-spinning process for UHMW-iPP fiber production.[6] However, extrusion for fiber spinning has not yet been reported for UHMW-iPP, probably caused by the inherent high melt viscosity impeding this process. Despite these difficult conditions, we isolated UHMW-iPP fibers of different molecular weights *via* melt extrusion and subsequently compared their mechanical properties to fibers of medium high molecular weight PP, both commercially available or received by homogeneous polymerization.

Results and Discussion

The list of iPP samples used for fiber spinning *via* melt extrusion in this study, ranging from medium high molecular weight to UHMW, is shown in Table 1. **iPP-1** was commercially available from *Ineos*, **iPP-2** to **iPP-5** were synthesized *via* single-site catalysis, using two literature known catalysts (Figure S45) –

Table 1. Tailored iPP for fiber spinning.

	M_w [kg/mol]	$Đ$ (–)	T_m [°C]	[mmmm][%]
iPP-1	330	6.6	162.8	95
iPP-2	380	2.4	157.7	94
iPP-3	860	1.8	165.6	>99
iPP-4	1200	1.8	165.4	>99
iPP-5	1400	1.8	165.5	>99

[a] *L. Stieglitz, P. F. Großmann, M. Kränzlein, K. Rodewald, Prof. B. Rieger*
Wacker-Lehrstuhl für Makromolekulare Chemie
Catalysis Research Center
TUM School of Natural Sciences
Technische Universität München
Lichtenbergstraße 4, 85748 Garching bei München (Germany)
E-mail: rieger@tum.de
[b] *C. Geiger, Prof. P. Müller-Buschbaum*
TUM School of Natural Sciences
Department of Physics
Technische Universität München
James-Franck-Straße 1, 85748 Garching (Germany)
[c] *Prof. P. Müller-Buschbaum*
Heinz Maier-Leibnitz Zentrum (MLZ)
Technische Universität München
Lichtenbergstraße 1, 85748 Garching (Germany)

Supporting information for this article is available on the WWW under https://doi.org/10.1002/cplu.202300045

iPP-2 was obtained by using **I**, and **II** was used for **iPP-3** to **iPP-5** combined with suitable polymerization conditions.[2c,7]

While **iPP-2** was received as a polymer powder, **iPP-3**–**iPP-5** were received as a fibrous material after synthesis. Therefore, these polymers were milled with an ultra-centrifugal mill to reduce the grain size. Chain destruction induced by oxidative stress during processing was avoided by applying an improved milling procedure (Figure S6–S10).

For subsequent fiber spinning, we combined a micro-compounder and a KPG-stirrer equipped with a manufactured spinning cone (Figure S24 and S25) – with this set-up (Figure 1, left), the spinning speed as well as the nozzle-cone distance could be adjusted to modify the fiber's diameter and ensure a solid phase. In preliminary experiments using a 0.50 mm spinning nozzle, it was shown that the commercial **iPP-1** has a good spinnability. The fiber's thickness could be adjusted arbitrarily up to 40 μm with no need for any stabilizing agent. In contrast to **iPP-1**, 1 wt% *Irganox* 1010 as stabilizing agent for UHMW-iPP could not prevent chain destruction and led to broadening of the polydispersity. Increasing the amount of *Irganox* to 3 wt% resulted in no spinnability and a checked-off extrudate. We therefore increased the nozzle's diameter to 2.00 mm – this resulted in a proper extrusion of the UHMW polymer. Screening for the appropriate amount of stabilizing agent revealed that the optimum amount is between 3 and 7 wt% (Figure S12). We decided to utilize the upper limit to avoid any chain destruction in the spinning or annealing process. To compare the mechanical properties of **iPP-1**–**iPP-5**, we used the same extrusion conditions and aimed for a fiber thickness of 200–400 μm, as, contrary to **iPP-1**, thin UHMW-iPP fibers were challenging to receive with our used set-up.

While spinning fine and thin fibers (40–120 μm) for **iPP-1** and **iPP-2** was comparably easy, an increase of the fiber's diameter turned out to be challenging when using the 0.50 mm fiber spinning nozzle. Therefore, we manufactured a 1.00 mm fiber spinning nozzle (Figure S23) combining the advantages of 0.50 mm fiber spinning and 2.00 mm extrusion nozzle: a smaller diameter as well as a longer nozzle distance for an improved homogeneity of the polymer melt. Still, this manufactured 1.00 mm nozzle was not useful for **iPP-3**–**iPP-5**, as the high melt viscosity of the polymers caused inhomogeneities and partially extrusion rupture, leading to no proper fiber spinning (Figure S30 and S41). After changing to the 2.00 mm extrusion nozzle, the extrusion of **iPP-3**–**iPP-5** was smooth (Figure S31, S34 and S38), melt spinning with only a few inhomogeneities (Figure S35 and S37) was accessible and UHMW fibers with a diameter of about 300 μm were received.

Figure 1. Set-up for fiber spinning (left) and agglutinated compounder (right) after spinning of UHMW-iPP.

After a few minutes in the compounder, the UHMW polymer's melt viscosity increased drastically, and extrusion ruptures occurred – yielding 2–4 cm long extrudates not suitable for melt spinning. However, with these molten extrudates, melt drawing instead of melt spinning was possible. This technique of post-extrusion drawing of as-spun fibers is applied e.g. by Kakiage et al. for fiber spinning of UHMW-PE fibers.[8] For this purpose, the molten extrudate with a diameter of 2.00 mm was stretched on both sides to a length of 20–30 cm with a stretching rate of 20 cm/sec. This consequently yielded a consistent fiber with a reduced diameter of 400 μm (Figure S33). After approximately ten minutes of the polymer inside the compounder, the UHMW polymer's melt agglutinated the compounder, and no extrusion was possible anymore (Figure 1, right). Adding new polymer or increasing the extrusion temperature up to 220 °C did not sufficiently reduce the agglutination. The removed polymer revealed no variation in the molecular weight, and after milling, the polymer remained non extrudable. Probably, the number of entanglements and consequently the polymer's melt viscosity were increased by the melting process and the arising shear forces, and therefore, the UHMW polymer was no longer extrudable.

DSC measurements of e.g. **iPP-5** support this hypothesis, as it was observed that the first melting transition and crystallinity (167.4 °C, 55.4 % crystallinity) is increased compared to the second transition (165.5 °C, 44.3 % crystallinity) – nevertheless, further investigations comparing the nascent, melt-crystallized and agglutinated polymer need to be conducted.

A mixture of 70 wt% **iPP-4** and 30 wt% **iPP-1** gave a smooth extrusion using the manufactured 1.00 mm fiber spinning nozzle with no observation of an increased melt viscosity or extrusion rupture. This yielded a composite fiber with a diameter of about 200 μm. Probably, combining two iPPs – one with a high and one with a low melt viscosity – is a promising method to avoid agglutination of the compounder.

Figure 2 illustrates the optical differences between the UHMW **iPP-4** and medium high molecular weight **iPP-1** fiber. Commercial **iPP-1** bearing a reduced melt viscosity and crystallinity enabled a very smooth and even fiber surface, whereas our UHMW-iPP with its ultrahigh molecular weight and increased crystallinity led to a high surface roughness induced by fibrillation. This high surface roughness is well known for UHMW-PE fibers, especially for high draw ratios.[11] Surprisingly, annealing of the polymer fibers melted the fiber surface for all investigated fibers (Figure 2). Underneath that melted surface, the fibrillated structure was preserved for UHMW fibers (Figure 2, b).

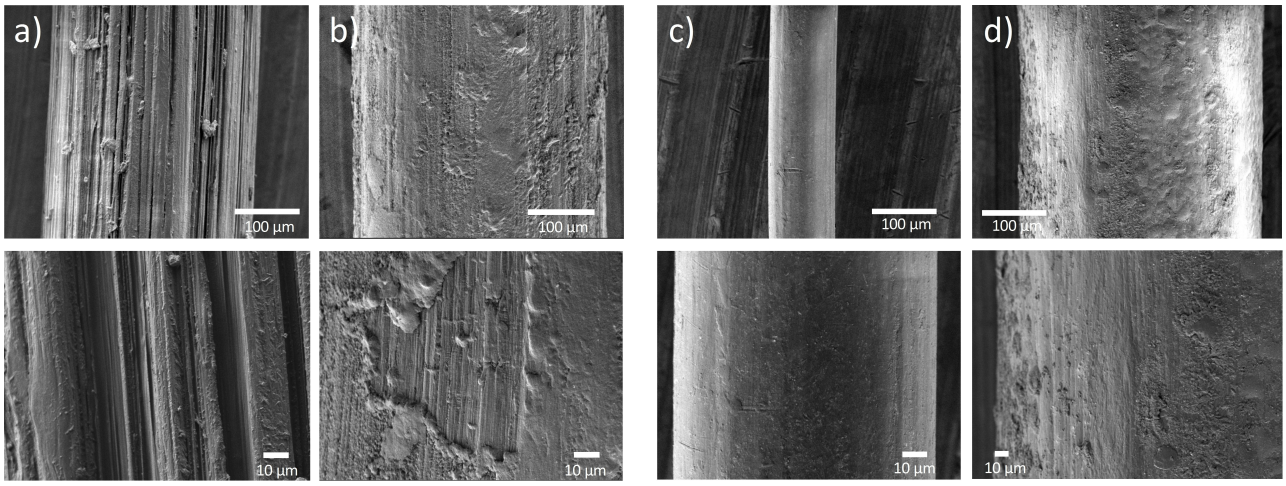

Figure 2. SEM images of a) melt drawn and b) annealed melt drawn **iPP-4** fiber compared to c) spun and d) annealed spun **iPP-1** fiber.

The mechanical properties of polymers, especially the tensile strength, highly depend on the crystallinity.[12] Besides increasing the isotacticity, annealing of the polymer is a commonly used technique to enhance the degree of crystallinity. In previous studies it was shown, that a higher annealing temperature leads to an increased crystallinity.[13] Furthermore, annealing prevents crazes and avoids coalescence, consequently improving the mechanical behavior.[13b] In preliminary experiments, an increased annealing temperature of 150 °C for 67 h turned out to be suited better for UHMW-iPP fibers compared to a temperature of 140 °C for 20 h (Figure S21 and S22). Actually, an even higher annealing temperature would be desirable, but due to an inaccurate temperature control this led to a partial melting of the polymer fibers. For **iPP-1** and **iPP-2** we reduced the annealing temperature to 143 °C, as 150 °C melted the polymer fibers.

The crystallization behavior of **iPP-5** during different stages of the fiber manufacturing process was analyzed by WAXS measurements (Figure 3). The crystalline fraction of the raw polymer sample consisted purely of the α-phase, which meets the expectation – it is reported that iPP from solution crystallization yields mostly the α-phase.[9] As expected for the raw polymer after precipitation synthesis without any further processing, there is no preferential orientation of the crystals, as seen from the uniform scattering intensity along the Debye-Scherrer rings. The extrudate still exhibited predominantly the α-phase for the crystalline fraction, but the formation of β-phase crystallites was detected as well. A weak preferential orientation of crystallites was observed. The sample exhibited a strong homoepitaxy[10] of the α-phase, identifiable by an intense (110)d reflex, originating from the daughter crystals, that were seen to orient roughly perpendicularly to the stretching direction, while the mother crystals orient roughly parallel to the stretching direction. In the spun fibers, the α-phase clearly predominated the crystalline fraction, but a small fraction of β-phase crystallites was still present (see Figure S44f). The crystallites in the spun fiber exhibited a strong preferential orientation. The sample, as already seen in the extrudate,

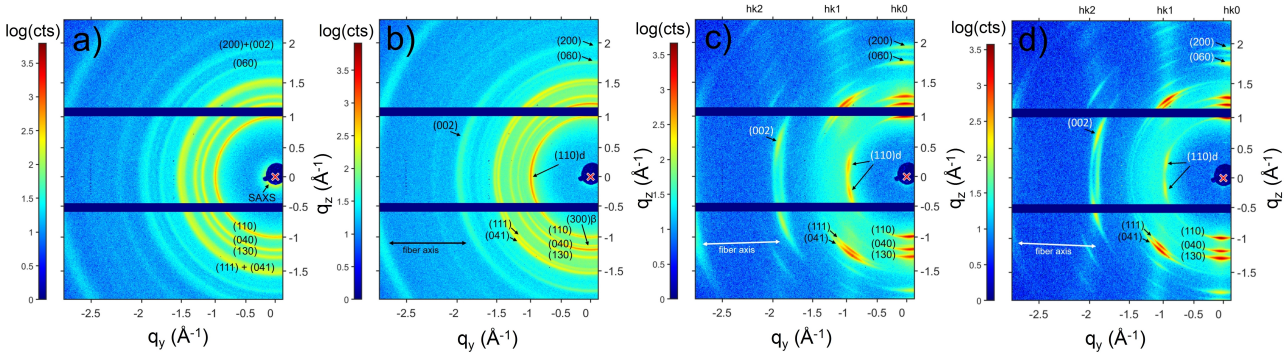

Figure 3. Transmission-mode WAXS data from UHMW **iPP-5** at different stages of the fiber fabrication process. a) raw polymer (obtained as fine mesh), b) extrudate, c) spun fiber, d) annealed fiber (fiber axis marked by arrow). Characteristic reflections belonging to the α-phase[9] of crystalline iPP predominantly found in all samples are marked with their corresponding *Miller* indices (exceptions are: (110)d marking the reflections of the daughter crystals resulting from iPP homoepitaxy[10] – all other indicated reflections belong to the mother crystals – and (300)β, marking the most intense reflection of the β-phase, seen most clearly in b) (extrudate)). A clear increase in preferential orientation of crystallites is seen from a) to d). Typical hk0 (equator) lines, hk1, and hk2 arcs, on which reflections sit, are marked for the spun and annealed fiber patterns in c) and d). Further information on WAXS measurements and data analysis is available in the Supporting Information.

showed a homoepitaxy of the α-phase, resulting in the (110)d daughter reflex appearing under the azimuthal angles 80° and 100° relative to the hk0 equator with the (110) mother reflex, as found in literature.[10] The separation of the daughter reflex is a result of the strong preferential orientation of all α-phase crystallites. A very similar scattering pattern was found in the annealed fiber as for the spun fiber. The main differences found were the depletion of the β-phase, which was no longer detectable, and the reduced intensity of the amorphous halo, as well as the increased sharpness (decreasing full width at half maximum (FWHM)) of the unique reflections of the α-phase.

We verified *via* GPC measurements (Figure 4, a), that neither the spinning process nor the annealing process led to bond breakage of the polymer fibers by an oxidative stress. Furthermore, we observed an increased melting transition temperature and crystallinity, especially after the annealing process, *via* DSC analysis (Figure 4, b), which is in agreement with the WAXS results. The degree of crystallinity was determined by using the melt enthalpy for polypropylene ΔH_{lit}, 100 % = 207 J/g.[11] Table 2 illustrates the influence of the

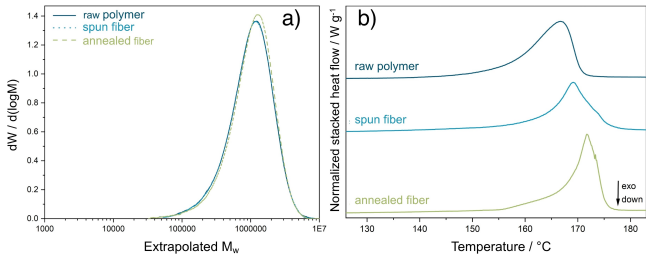

Figure 4. GPC (a) and DSC (b) analysis of **iPP-4**.

Table 2. Calculated Crystallinity *via* DSC analysis.

	iPP-1	iPP-2	iPP-3	iPP-4	iPP-5
raw	44.6 %	41.4 %	44.1 %	43.9 %	44.3 %
spun fiber	47.0 %	43.2 %	45.6 %	48.1 %	46.8 %
annealed fiber	50.1 %	46.0 %	53.0 %	52.2 %	53.5 %

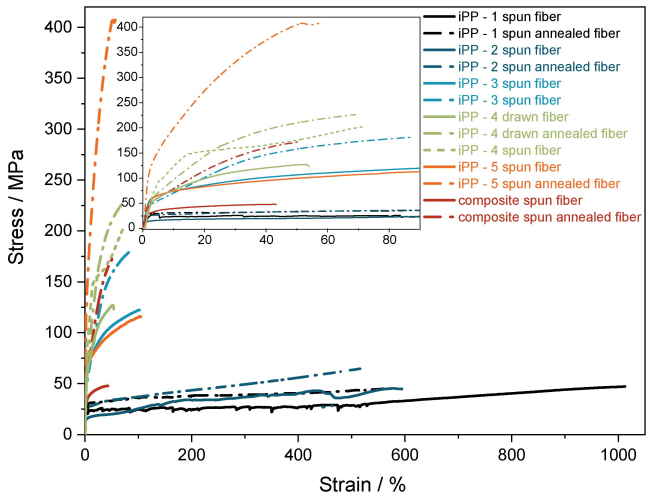

Figure 5. Stress strain mechanical behavior of spun and annealed fibers.

crystallite orientation induced by fiber spinning and increased lamellae thickness by the annealing process.

Examining their mechanical behavior *via* stress strain measurements, the extraordinary potential of UHMW-iPP fibers compared to fibers manufactured from industrially available iPP is highlighted (Figure 5). All UHMW-iPP fibers, due to their higher molecular weight and lower polydispersity, exhibited a higher tensile strength and a shortened elongation at break compared to the *Ziegler-Natta* based **iPP-1**.[14] The increase in crystallinity (Table 2) induced by the annealing process boosted the tensile strength of all polymer fibers **iPP-1**–**iPP-5** (e.g. **iPP-5** spun and annealed fiber, Figure 5) and a tensile strength of up to 400 MPa was received for UHMW-iPP fibers. The melt drawing process of **iPP-4** however yielded a decreased tensile strength compared to the melt spinning process – probably due to inhomogeneities in the molten extrudate. The composite fiber of 70 wt% **iPP-4** and 30 wt% **iPP-1** surprisingly showed a low tensile strength combined with a low elongation at break – despite the high amount of UHMW-iPP in the feedstock material. Presumably, the two different polymers were not evenly distributed in the composite polymer fiber, leading to defects and an overall deteriorated mechanical behavior. During the annealing process, defects in the composite structure are reduced and the crystalline fraction increased (see Figure S44), thus improving the stress strain behavior. Blending UHMW-iPP with an iPP bearing a lower melt viscosity not only avoids agglutination of the compounder, but also is a promising method to obtain strong iPP fibers. Clearly, this presented technique yields lower tensile strengths and an increased fiber's diameter compared to previous reported UHMW-iPP fibers accessed by gel-spinning[6a,c,d] – however, this study highlights, that extrusion of UHMW-iPP is feasible and thus may pave the way for an improved spinning technique of UHMW-iPP.

Conclusion

In summary, we performed melt spinning and melt drawing of various iPP samples, including the first reported extrusion processing of UHMW-iPP. We investigated the crystallinity and phase crystallization *via* DSC and WAXS analysis and confirmed no chain breakage occurring during the spinning process. We proved that UHMW-iPP fibers enable a high tensile strength that was even increased after an annealing process (up to 400 MPa). However, UHMW-iPP exhibited a short melt spinning time window due to its increasing melt viscosity – after that, no spinning was possible at all. Nevertheless, by mixing a lower molecular weight iPP fraction to the feedstock, extrusion rupture and agglutination of the compounder was avoided and a composite fiber with enhanced mechanical properties was obtained. As these findings are very promising, further studies need to be conducted to better understand the root cause of the agglutination and increased melt viscosity and also to improve the mechanical properties of the obtained fibers.

Experimental Section

Polymer ^{13}C NMR spectra were measured with an ARX-300 spectrometer at 140 °C in bromobenzene-d^5 with 40–60 mg/mL and 14k scans with 5 mm OD tubes. Acquisition conditions were: 30° flip angle; 1.82 sec acquisition time, 2 sec relaxation delay. Broadband proton decoupling was achieved with a WALTZ16 sequence. The degree of isotacticity was determined via the integration of the corresponding [mmmm]-pentade (21.85 ppm)[15] against the region of 19.5–22.5 ppm.

Gel permeation chromatography (GPC) was performed with a PL-GPC 220 instrument equipped with 2x Olexis 300 mm × 7.5 mm columns and triple detection via a differential refractive index detector, a PL-BV 400 HT viscometer, and light scattering (Precision Detectors Model 2040, 15 and 90°). Measurements were performed at 160 °C using HPLC-grade 1,2,4-trichlorobenzene (TCB; 100 mg/L BHT) from Sigma-Aldrich with a constant flow rate of 1 mL/min and a calibration set with narrow-MWD polyethylene (PE) and polystyrene (PS) standards. Samples were prepared by dissolving 0.5–0.7 mg of the polymer in 1.0 mL of stabilized TCB for 1 h at 140 °C immediately before each measurement. The molecular weight was determined absolutely against PS standards by using dn/dc = 0.097 mL/g.[16]

Differential scanning calorimetry (DSC) analysis was conducted on a DSC Q2000 instrument from TA Instruments. The polymer (4–5 mg) was sealed into a non-hermetic aluminum pan and heated from 50 to 200 °C at 10 °C/min. After the temperature was held for 2 min, the sample was cooled to 50 °C at 10 °C/min and heated again in the same manner. The reported values for raw polymers are those determined in the second heating cycle, for fibers those determined in the first heating cycle.

Optical light microscopy was carried out using a PantheraTEC-BD from Motic equipped with a MicroCam II camera from Bresser. The software MicroCamLabII was used for processing.

The surface of the fibers was determined by the images taken by JEOL JSM-7500F field-emission scanning electron microscope coupled with EDX INCA System (software) with 50 mm^2 X-MAX detector from Oxford Instruments.

As **iPP-3**–**iPP-5** were received as a fibrous material, these polymers had to be milled for an extrusion processing. The coarsely crushed polymer was frozen in liquid nitrogen and subsequently milled chunkwise by using a *Retsch ultra centrifugal mill ZM 200* (12-tooth rotor, sieve size 2.00 mm, trapezoid holes) at 1000 rpm.

Extrusion for fiber spinning was conducted using a Micro-Compounder from *DACA Instruments*. The temperature was set at 195 °C and 7% wt. of the stabilizing agent *Irganox 1010* added to the polymer prior the extrusion. 2–2.5 g of the stabilized polymer were added to the compounder and after an appropriate mixing time (for iPP-1 and iPP-2 three minutes, for iPP-3–iPP-5 15 seconds) the extrusion was initiated. The molten extrudate was rolled onto the manufactured spinning cone's rod (Figure S24 and S25) – when the fiber's diameter was smooth, the spinning was conducted on the spinning cone. With the attached *Heidolph* KPG-stirrer, the distance between nozzle and cone and spinning speed was adjusted according to the desired fiber characteristics and polymer's melt viscosity. An increased KPG stirring speed gave a thinner polymer fiber, but the distance between nozzle and cone had to be increased to ensure an entire solidification of the fiber.

Acknowledgements

The authors particularly thank Zwick Roell GmbH & Co. KG for the provided stress-strain measurements of the polymer fibers. Furthermore, we thank Dr. Thomas Pehl, Tim Lenz and Jonas Bruckmoser for valuable discussions. Open Access funding enabled and organized by Projekt DEAL.

Conflict of Interest

The authors declare no conflict of interest.

Data Availability Statement

The data that support the findings of this study are available from the corresponding author upon reasonable request.

Keywords: fiber spinning · isotactic polymers · polypropylene · tensile strength · ultrahigh molecular weight

[1] W. Kaminsky, K. Külper, H. H. Brintzinger, F. R. W. P. Wild, *Angew. Chem. Int. Ed. Engl.* **1985**, *24*, 507–508.
[2] a) A. Schöbel, E. Herdtweck, M. Parkinson, B. Rieger, *Chem. Eur. J.* **2012**, *18*, 4174–4178; b) M. R. Machat, C. Jandl, B. Rieger, *Organometallics* **2017**, *36*, 1408–1418; c) M. R. Machat, D. Lanzinger, A. Pöthig, B. Rieger, *Organometallics* **2016**, *36*, 399–408; d) M. R. Machat, A. Fischer, D. Schmitz, M. Vöst, M. Drees, C. Jandl, A. Pöthig, N. P. M. Casati, W. Scherer, B. Rieger, *Organometallics* **2018**, *37*, 2690–2705; e) P. S. Kulyabin, G. P. Goryunov, M. I. Sharikov, V. V. Izmer, A. Vittoria, P. H. Budzelaar, V. Busico, A. Z. Voskoboynikov, C. Ehm, R. Cipullo, *J. Am. Chem. Soc.* **2021**, *143*, 7641–7647; f) W. Spaleck, M. Antberg, J. Rohrmann, A. Winter, B. Bachmann, P. Kiprof, J. Behm, W. A. Herrmann, *Angew. Chem. Int. Ed. Engl.* **1992**, *31*, 1347–1350; g) W. Spaleck, F. Kueber, A. Winter, J. Rohrmann, B. Bachmann, M. Antberg, V. Dolle, E. F. Paulus, *Organometallics* **1994**, *13*, 954–963; h) G. P. Goryunov, M. I. Sharikov, A. N. Iashin, J. A. M. Canich, S. J. Mattler, J. R. Hagadorn, D. V. Uborsky, A. Z. Voskoboynikov, *ACS Catal.* **2021**, *11*, 8079–8086; i) V. V. Izmer, A. Y. Lebedev, D. S. Kononovich, I. S. Borisov, P. S. Kulyabin, G. P. Goryunov, D. V. Uborsky, J. A. M. Canich, A. Z. Voskoboynikov, *Organometallics* **2019**, *38*, 4645–4657; j) P. S. Kulyabin, V. V. Izmer, G. P. Goryunov, M. I. Sharikov, D. S. Kononovich, D. V. Uborsky, J. A. M. Canich, A. Z. Voskoboynikov, *Dalton Trans.* **2021**, *50*, 6170–6180; k) A. Vittoria, G. P. Goryunov, V. V. Izmer, D. S. Kononovich, O. V. Samsonov, F. Zaccaria, G. Urciuoli, P. H. Budzelaar, V. Busico, A. Z. Voskoboynikov, *Polymer* **2021**, *13*, 2621.
[3] L. Stieglitz, T. M. Lenz, A. Saurwein, B. Rieger, *Angew. Chem. Int. Ed.* **2022**, *61*, e202210797.
[4] R. Marroquin-Garcia, N. Leone, L. G. D. Hawke, D. Romano, C. H. R. M. Wilsens, S. Rastogi, *Macromolecules* **2022**, *55*, 2574–2587.
[5] R. H. Colby, L. J. Fetters, W. W. Graessley, *Macromolecules* **1987**, *20*, 2226–2237.
[6] a) C. Bastiaansen, P. Lemstra, in *Makromolekulare Chemie. Macromolecular Symposia, Vol. 28*, Wiley Online Library, **1989**, pp. 73–84; b) M. Matsuo, T. Hashida, K. Tashiro, Y. Agari, *Macromolecules* **2002**, *35*, 3030–3040; c) T. Ogita, Y. Kawahara, Y. Soga, M. Matsuo, *Colloid Polym. Sci.* **1992**, *270*, 833–839; d) Y. Ikeda, T. Ohta, *Sen'i Gakkaishi* **2002**, *58*, 444–450.
[7] L. Stieglitz, D. Henschel, T. Pehl, B. Rieger, *Organometallics* **2021**, *40*, 4055–4065.
[8] a) M. Kakiage, D. Fukagawa, *Mater. Today Commun.* **2020**, *23*, 100864; b) M. Kakiage, S. Takei, *Macromol. Mater. Eng.* **2020**, *305*, 2000252.
[9] A. T. Jones, J. M. Aizlewood, D. R. Beckett, *Makromol. Chem.* **1964**, *75*, 134–158.

[10] T. Raidt, R. Hoeher, F. Katzenberg, J. C. Tiller, *Macromol. Rapid Commun.* **2015**, *36*, 744–749.
[11] E. Wölfel, H. Brünig, I. Curosu, V. Mechtcherine, C. Scheffler, *Materials* **2021**, *14*, 722.
[12] A. Galeski, *Prog. Polym. Sci.* **2003**, *28*, 1643–1699.
[13] a) T. Parenteau, G. Ausias, Y. Grohens, P. Pilvin, *Polymer* **2012**, *53*, 5873–5884; b) P. Frontini, A. Fave, *J. Mater. Sci.* **1995**, *30*, 2446–2454.
[14] S. Misra, F.-M. Lu, J. E. Spruiell, G. C. Richeson, *J. Appl. Polym. Sci.* **1995**, *56*, 1761–1779.
[15] H. H. Brintzinger, D. Fischer, R. Mülhaupt, B. Rieger, R. M. Waymouth, *Angew. Chem. Int. Ed. Engl.* **1995**, *34*, 1143–1170.
[16] B. Coto, J. M. Escola, I. Suárez, M. J. Caballero, *Polym. Test.* **2007**, *26*, 568–575.

Manuscript received: January 23, 2023
Revised manuscript received: February 9, 2023
Accepted manuscript online: February 14, 2023